*sustainability*

MDPI

*Article*

# Evaluation Study on a Novel Structure CCHP System with a New Comprehensive Index Using Improved ALO Algorithm

**Jie Ji [1,*], Fucheng Wang [1], Mengxiong Zhou [1], Renwei Guo [1], Rundong Ji [2], Hui Huang [1], Jiayu Zhang [1], Muhammad Shahzad Nazir [1], Tian Peng [1], Chu Zhang [1], Jiahui Huang [1] and Yaodong Wang [3]**

[1] Electric Engineering Department, Automatic Faculty, Huaiyin Institute of Technology, Huaiyin 223002, China
[2] Jiangsu Huashui Engineering Detection & Consulting Co., Ltd., Huai'an 223001, China
[3] Department of Engineering, Durham Energy Institute, Durham University, Durham DH1 3LE, UK
* Correspondence: jijie@hyit.edu.cn

**Abstract:** The CCHP system is a reasonable and effective method to improve the current situation of energy use. Capacity allocation is of great significance in improving the performance of the CCHP system. Due to the particularity of chemical enterprises' production process, the demand for cooling, heating, and power load is also relatively particular, which makes the dynamic loads challenging to be satisfied. Because of the above problems, the structure of the typical CCHP system is improved, embodied in the collocation of multi-stage lithium bromide chiller, and the use of various energy storage devices. Based on the improved ant lion intelligent optimization (ALO) algorithm, the comprehensive evaluation index coupled with energy benefit, economic benefit, and environmental benefit, is taken as the objective function, and the equipment capacity configuration of the CCHP system for chemical enterprises is studied. Considering winter, summer, and transition seasons, the results show that the system is better than the typical CCHP system. The annual cost savings of the new structural system are up to 13%, and the carbon dioxide emissions of the new structural system are reduced by up to 36.39%. The primary energy utilization rate of the new structure system is increased by 18%, and the comprehensive evaluation index also performs better. The optimal index can reach 0.814.

**Keywords:** CCHP; capacity configuration; energy system; accumulated energy; ALO

check for updates

**Citation:** Ji, J.; Wang, F.; Zhou, M.; Guo, R.; Ji, R.; Huang, H.; Zhang, J.; Nazir, M.S.; Peng, T.; Zhang, C.; et al. Evaluation Study on a Novel Structure CCHP System with a New Comprehensive Index Using Improved ALO Algorithm. *Sustainability* **2022**, *14*, 15419. https://doi.org/10.3390/su142215419

Academic Editor: Md. Hasanuzzaman

Received: 11 October 2022
Accepted: 17 November 2022
Published: 20 November 2022

**Publisher's Note:** MDPI stays neutral with regard to jurisdictional claims in published maps and institutional affiliations.

**Copyright:** © 2022 by the authors. Licensee MDPI, Basel, Switzerland. This article is an open access article distributed under the terms and conditions of the Creative Commons Attribution (CC BY) license (https://creativecommons.org/licenses/by/4.0/).

## 1. Introduction

China is the largest energy consumer, and coal occupies an absolute position in all kinds of energy consumption in China. A large amount of coal investment and utilization contradicts human development [1]. As a distributed energy system, the CCHP system can provide a solution to reduce fossil energy and clean energy use. Research on the CCHP systems is of great significance in promoting energy efficiency, economic benefits, and environmental benefits of the system.

Domestic and foreign scholars have studied the CCHP system coupled with clean energy. Regarding the structure of the CCHP system, Meng et al. [2] verified through the thermodynamic model that a CCHP system using an internal combustion engine with natural gas as the power system had a higher utilization efficiency of primary energy. Li et al. [3], through the control variable method, used the evaporation temperature as a single variable to verify the biomass-driven CCHP system in the four modes of economic optimal. Zhang et al. [4] demonstrated that a CCHP system with photovoltaic power generation had better economic and environmental benefits through mixed binary particle swarm optimization based on niche. For the existing CCHP system with an internal combustion engine as a power plant, the low energy utilization rate and large equipment volume are contrary to the high flexibility CCHP system. For the CCHP system with photovoltaic coupling, the coupling energy storage unit is not considered, and the intermittent energy

supply problem is prone to occur. Presently, various bromide chillers have not been used in cascade, and the system structure of heat in the process is fully utilized.

For the CCHP system's research, the system capacity draws attention. Wei et al. [5] studied the photovoltaic model and the CCHP system model through a niche [6] particle swarm optimization algorithm and fuzzy ideal decision, optimized the capacity configuration of photovoltaic and CCHP systems, and verified its feasibility to obtain satisfactory results. Zhang et al. [7], through the principle of energy balance, established a mixed integer nonlinear programming model of integrated energy systems, including production, recovery, conversion, and storage. The author further explored the applicability of system capacity allocation in different regions and environments, and obtained satisfactory results. Li et al. [8] took a regional energy supply project in Shanghai as an example and analyzed the relationship between generator capacity and different sizes and grid connection modes. It was considered that the generators' ability in the triple power supply system depends on comprehensive factors such as system load, energy price, energy policy, and initial investment. It cannot be directly applied to the traditional cogeneration by heat to determine electricity or heat. Xu et al. [9], by analyzing the system's environmental, energy, and exergy benefits, found the optimal size of the prime mover, verified the system's reliability, and obtained satisfactory results. Wu et al. [10] explored the research system through an exhaustive search algorithm and cost-oriented index optimization method to determine the optimal configuration of the system. For the existing CCHP system, involving equipment capacity configuration research, it is not conducive to only consider specific situations.

The optimal operation study [11] is significant for a complex energy system's overall performance. In terms of the evaluation of the energy system, Mianaei et al. [12] established an overall operating cost of the evaluation system to obtain the minimum cost. Cao et al. [13] established an evaluation system of coupling annual cost savings, immediate energy savings, and the rate of carbon dioxide emission reductions. The coupling mode is to add equal weight. Wang et al. [14] established the evaluation system of the coupling of the annual system cost, pollution gas emissions, and primary energy consumption, and the coupling mode is to add equal weight. The existing evaluation system is divided into single-objective and multi-objective evaluation by weight coupling. The former is not comprehensive enough for the selection of evaluation objectives, and it is easy to sacrifice other indicators to improve the selected indicators. Although the latter comprehensively considers three seed indicators, the coupling method is not appropriate, and it cannot be considered by equal weight, which requires more proper selection.

This paper mainly studies the application of combined a cooling, heating, and power supply system coupled with photovoltaic in a chemical enterprise in the Huai'an area. According to target demand, the equipment capacity of the system is configured. Taking the comprehensive evaluation system as the objective function, the intelligent optimization algorithm is used to flexibly adjust the equipment capacity configuration, which includes three aspects:

1. The photovoltaic power generation model is established according to the meteorological data of solar irradiance and sunshine hours in the Huai'an area, and the photovoltaic power generation curve is obtained. Combined with a chemical enterprise's cooling, heating, and power load demand curve, the input data of the cooling, heating, and electricity demand are formed.
2. A novel CCHP model is constructed, and the overall equipment model is established. The essential parts are finely modeled, and the capacity of the equipment is configured. Considering the annual operation of the system, the operating condition curve is output.
3. A comprehensive evaluation system is established and used as the objective function. The intelligent optimization algorithm is used to optimize the equipment capacity configuration to flexibly adjust the optimal equipment capacity in the system's operation.

In this paper, the overall research road-map is shown in Figure 1:

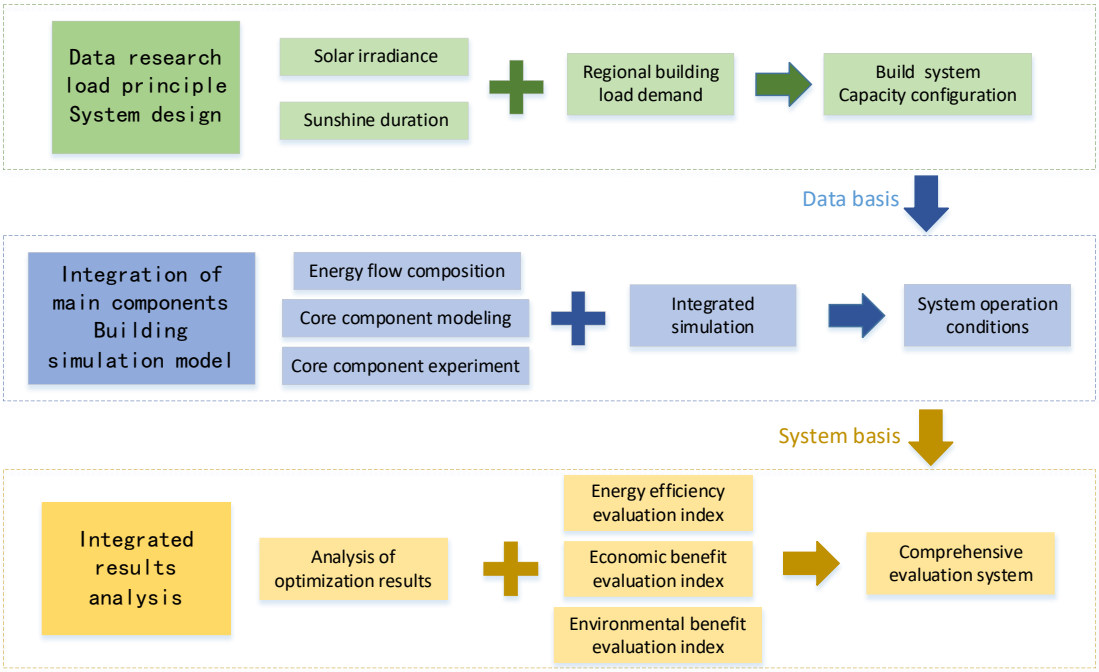


**Figure 1.** Overall research road-map.

## 2. Methods

### *2.1. Energy Flow in CCHP System*

Cooling load: cooling capacity of electric refrigerator + cooling capacity of waste heat lithium bromide absorption chiller + cooling capacity of steam dual-effect lithium bromide absorption chiller = building cooling demand [15]:

$$Q^{c}_{EC} + Q^{c}_{AC.W} + Q^{c}_{AC.S} = Q^{c} \quad (1)$$

where $Q^{c}_{EC}$ is the refrigerating capacity of the electric refrigerator, $Q^{c}_{AC.W}$ is the refrigerating capacity of the waste heat lithium bromide absorption chiller, $Q^{c}_{AC.S}$ is the refrigerating capacity of the steam dual-effect lithium bromide absorption chiller, and $Q^{c}$ is the cooling demand of the building.

Heating load: gas turbine heat = heat required for waste heat lithium bromide absorption chiller + heat recovery from boiler + heat recovery from heat exchanger:

$$Q^{h}_{GT} = Q^{h}_{AC.W} + Q^{h}_{WHRB} + Q^{h}_{HEX} \quad (2)$$

where $Q^{h}_{GT}$ is the heat of gas turbine, $Q^{h}_{AC.W}$ is the heat required for waste heat lithium bromide absorption chiller, $Q^{h}_{WHRB}$ is the heat recovered from the boiler, and $Q^{h}_{HEX}$ is the heat recovered from the heat exchanger.

Heating Supply of Electric Boiler + Heating Supply of Exchanger + Heating Supply of Recovery Boiler = Building Heating Demand

$$Q^{h}_{EB} + Q^{h}_{HEX} + Q^{h}_{WHRB} = Q^{h} \quad (3)$$

Among them, $Q^{h}_{EB}$ is the heat production of electric boiler, $Q^{h}_{HEX}$ is the heat supply of heat exchanger, $Q^{h}_{WHRB}$ is the heat recovery boiler, $Q^{h}$ is the building heat demand.

Electric load: photovoltaic array power generation + gas turbine power generation = electric refrigerator power + electric boiler power + building electricity demand:

$$E^{i}_{PV} + E^{i}_{GT} = E^{i}_{EC} + E^{i}_{EB} + E^{i} \quad (4)$$

Among them, $E_{PV}^{i}$ is photovoltaic array power generation, $E_{GT}^{i}$ is gas turbine power generation, $E_{EC}^{i}$ is electric refrigerator power consumption, $E_{EB}^{i}$ is electric boiler power consumption, $E^{i}$ is building electricity demand.

The specific energy flow diagram is shown in Figure 2.

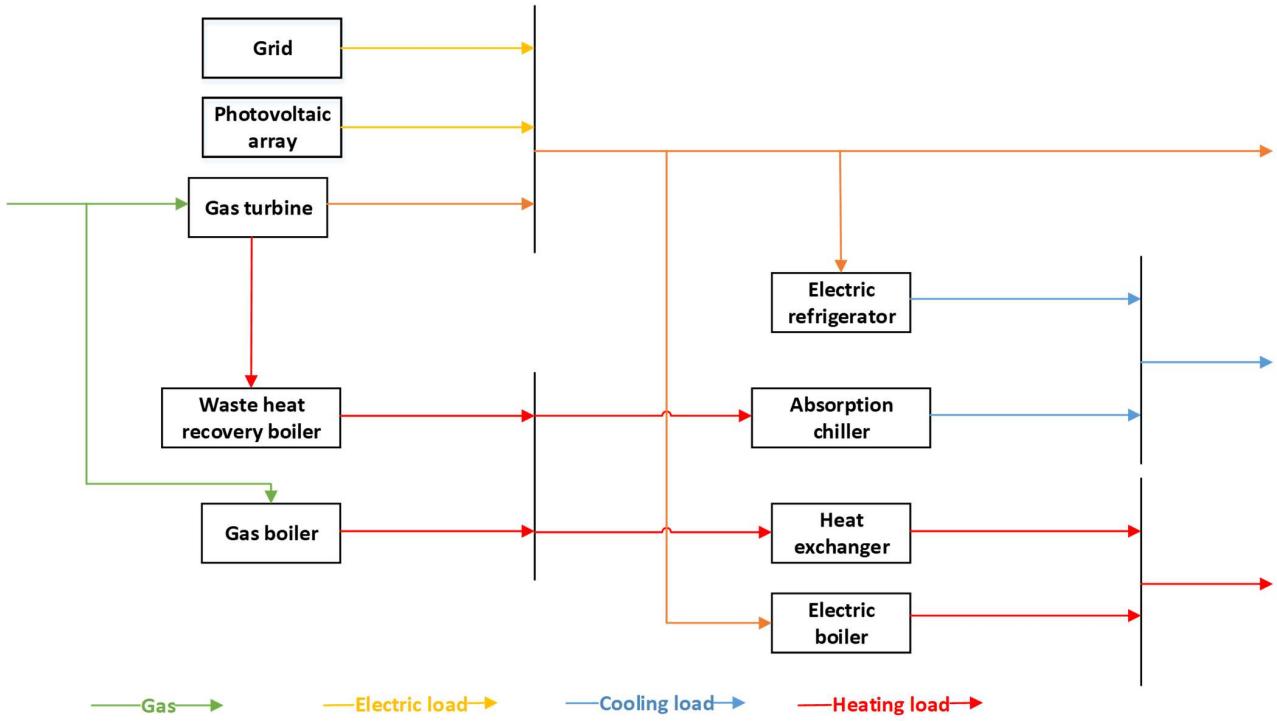


**Figure 2.** Energy flow.

### 2.2. Structure of CCHP System

To realize the coupling and clean energy of the CCHP system, the following CCHP model is established. The energy input includes natural gas and solar power [16]. The system structure consists of a gas turbine, gas boiler, heat recovery boiler, heat exchanger, waste heat lithium bromide absorption chiller, steam double effect lithium bromide absorption chiller, flue gas condensation heat exchanger, photovoltaic array, electric refrigerator, electric boiler, and energy storage device [17]. The operation method of the system is as follows: natural gas as fuel for gas boiler and gas turbine, supply system electric load and heat load for power generation device, photovoltaic array uses solar energy to supply system electric load; the heat generated by the gas turbine enters the heat recovery boiler [18] to deliver the heat load of the system, the cylinder water of the gas turbine supplies the heat load of the system through the heat exchanger, and the electric boiler supplies the heat load of the system. The waste heat lithium bromide absorption chiller uses the flue gas generated by the gas turbine to supply the cooling load of the system, the steam dual-effect lithium bromide absorption chiller uses the heating boiler as the heat source to supply the cooling load of the system, and the electric refrigeration unit supplies the cooling load of the system. For the heat load, the priority of the heat recovery boiler is greater than that of the gas boiler; for the cooling load, the priority of waste heat lithium bromide absorption chillers and steam double-effect lithium bromide absorption chillers using heat is greater than that of electric chillers. The specific system structure is shown in Figure 3.

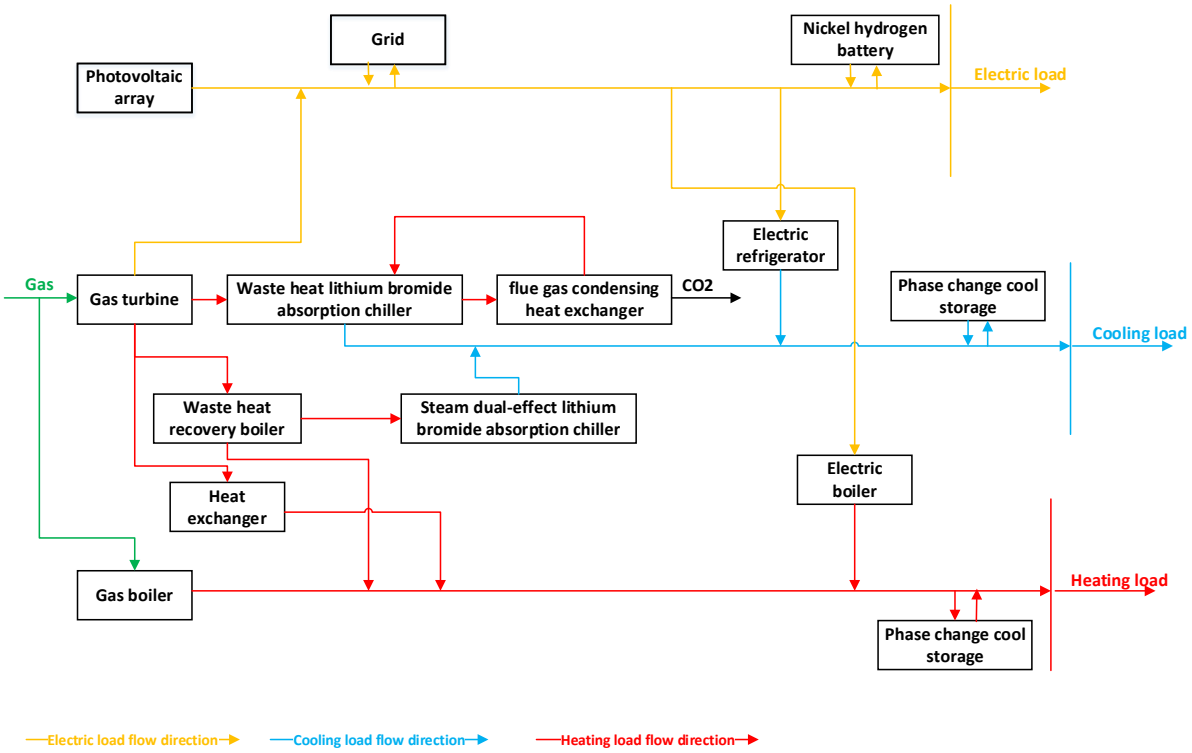


**Figure 3.** Structure diagram of CCHP system.

#### 2.2.1. Gas Turbine (GT)

While generating electricity, gas turbines can recover and utilize the heat they generate for heating or driving other equipment. Gas turbine power generation can be expressed as [19]:

$$E_{GT}^{i} = F_{GT} \cdot \eta_e \tag{5}$$

where $F_{GT}$ is the energy consumed by gas turbine power generation, and $\eta_e$ is the power generation efficiency of gas turbine.

#### 2.2.2. Gas Boiler (GB)

Gas boiler has the characteristics of high thermal efficiency and low environmental pollution. Its output characteristics depend on its performance and load demand. The output heating capacity can be expressed as [10]:

$$Q_{GB}^{h} = F_{GB} \cdot \eta_{GB} \tag{6}$$

Among them, $F_{GB}$ is the energy consumed by gas boiler, $\eta_{GB}$ is the efficiency of gas boiler.

#### 2.2.3. Electric Refrigerator (EC)

The refrigeration characteristics of the electric refrigerator are related to the refrigeration coefficient of the equipment. The output refrigeration capacity can be expressed as [20]:

$$Q_{EC}^{c} = E_{EC}^{i} \cdot COP_{EC} \tag{7}$$

where $COP_{EC}$ is the refrigeration performance coefficient of the electric refrigerator.

2.2.4. Waste Heat Lithium Bromide Absorption Chiller (AC.W)

Waste heat lithium bromide absorption chiller uses waste heat to drive lithium bromide chiller for energy supply. Its output efficiency is related to waste heat utilization rate and the waste heat refrigeration rate. The output refrigeration capacity can be expressed as:

$$Q^c_{AC.W} = Q^h_{GT} \cdot COP_{AC.W} \tag{8}$$

$$\eta = \frac{Q_{use}}{Q_{total}} = \frac{T_{in} - T_{out}}{T_{in} - T_o} \tag{9}$$

where $COP_{AC.W}$ is the refrigeration performance coefficient of the waste heat lithium bromide absorption chiller, $\eta$ is the waste heat utilization rate, $Q_{use}$ is the waste heat utilization amount; $Q_{total}$ is the total waste heat, $T_{in}$ is the inlet temperature of flue gas; $T_{out}$ is the exhaust temperature; and $T_o$ is the ambient temperature.

2.2.5. Steam Dual-Effect Lithium Bromide Absorption Chiller (AC.S)

The output characteristics of the steam double-effect lithium bromide absorption chiller are related to the fluctuation of steam pressure. The output refrigerating capacity can be expressed as:

$$Q^c_{AC.S} = Q^h_{WHRB} \cdot COP_{AC.S} \tag{10}$$

where $COP_{AC.S}$ is the refrigeration performance coefficient of the steam dual-effect lithium bromide absorption chiller.

2.2.6. Waste Heat Recovery Boiler (WHRB)

The heat recovery boiler makes use of the sensible heat in the waste gas, waste material or waste liquid in various industrial processes and the heat generated by the combustion of combustible materials to heat. The heat output can be expressed as [21]:

$$Q^h_{WHRB} = F_{GT} \cdot \eta_{rec} \cdot (1 - \eta_e) \tag{11}$$

where $\eta_{rec}$ is the heat recovery efficiency.

2.2.7. Photovoltaic Array (PV)

A photovoltaic array is the connection of multiple photovoltaic cells. Solar energy is converted into DC energy by photovoltaic cells. The output of the photovoltaic array is the inverter. The adaptation of the inverter should be considered when designing a photovoltaic array. The output power can be expressed as [22]:

$$I = I_{sc}\left\{1 - C_1\left[\exp\left(\frac{U}{C_2 U_{oc}}\right) - 1\right]\right\} \tag{12}$$

$$C_1 = \frac{I_0}{I_{sc}} \tag{13}$$

$$C_2 = \left(\ln\left(\frac{1}{C_1} + 1\right)\right)^{-1} \tag{14}$$

Among them, $I$ is output current, $I_{sc}$ is short circuit current, $U$ is output voltage, $U_{oc}$ is open circuit voltage, $I_0$ is diode reverse saturation current, $C_1$ and $C_2$ are the process variable.

2.2.8. Electric Boiler (EB)

Electric boiler converts electric power into heat energy. The output of steam and high temperature water with heat energy can be expressed as:

$$Q^h_{EB} = E^i_{EB} \cdot \eta_{EB} \tag{15}$$

where $\eta_{EB}$ is electric boiler efficiency.

2.2.9. Heat Exchanger (HEX)

A heat exchanger is often used to heat a low-temperature fluid or cool a high-temperature fluid in chemical and other industrial production. Its output can be expressed as [23]:

$$Q_{HEX}^{h} = Q_{GT}^{h} \cdot \eta_{HEX} \tag{16}$$

where $\eta_{HEX}$ is heat exchanger efficiency.

## 3. Capacity Configuration Optimization Model

In this paper, the system capacity is configured through a local chemical enterprise's typical daily load demand in winter and summer [24]. The system equipment capacity is optimized through the established comprehensive evaluation system. Under the premise of meeting the load demand of the enterprise, the optimal equipment capacity in the system's operation is flexibly adjusted.

### *3.1. System Capacity Configuration Aiming at Demand*

According to the load demand of chemical enterprises, allocating equipment capacity with capacity is carried out. Considering various factors of chemical enterprises and combining them with the expected target of the system, an inductive analysis is carried out. The system equipment capacity is preliminarily configured, and the equipment capacity is flexibly adjusted according to the optimization algorithm. System capacity configuration achieves refrigeration, heating, and the supply of various energy sources for power generation conforms to the actual demand.

### *3.2. Comprehensive Evaluation System*

3.2.1. Annual Cost

The annual cost method is the most commonly used dynamic economic evaluation method, including three parts: investment cost, operation cost and maintenance cost, which can be expressed as [25]:

$$ATC = C_i + C_o + C_m \tag{17}$$

where $ATC$ is the annual cost, $C_i$ is the investment cost, $C_o$ is the operation cost, $C_m$ is the maintenance cost.

**(1) Investment Cost**

The investment cost is the cost of the energy system purchase equipment, which can be expressed as [26]:

$$C_i = [R(1 - v) + iv] \times \sum_{k=1}^{l} N_k C_k \tag{18}$$

$$R = i(1 + i)^n / \left[(1 + i)^n - 1\right] \tag{19}$$

where $C_i$ is the investment cost, $R$ is the investment recovery coefficient, $v$ is the residual rate, $i$ is the annual interest rate, $N_k$ is the kth equipment capacity, $C_k$ is the initial investment of the kth equipment capacity, $l$ is the total number of system equipment, and $n$ is the life span of equipment.

**(2) Operation Cost**

Operating cost refers to the energy cost of the energy system directly consuming natural gas and other input energy, which can be expressed as:

$$C_o = \sum_{i=1}^{8760} \left(F_{GT} C_{gas} + F_{GB} C_{gas}\right) \tag{20}$$

where $C_o$ represents operating costs, $C_{gas}$ represents natural gas prices, $F_{GT}$ is the energy consumed by gas turbine power generation, $F_{GB}$ is the energy consumed by gas boiler.

**(3) Maintenance Cost**

Maintenance costs include equipment maintenance costs, regular inspection and daily maintenance costs, which can be expressed as:

$$C_m = \varepsilon \times C_i \tag{21}$$

where $C_m$ is the maintenance cost, $\varepsilon$ is proportional coefficient.

3.2.2. Primary Energy Ratio

The primary energy utilization rate is the ratio of the output energy of the system to the primary energy consumption. The output energy is combined with three kinds of load supply, and the primary energy consumption is the energy consumed by gas turbine and the gas boiler. It can be expressed as:

$$PER = \frac{E^i + Q^c + Q^h}{F_{GT} + F_{GB}} \tag{22}$$

3.2.3. Carbon Dioxide Emissions

Pollutants will be generated in the operation of the energy system. The emission of $CO_2$ is a crucial issue of world concern, and it is also the research object commonly used in the energy system. Therefore, the emission of $CO_2$ is regarded as the evaluation standard of environmental indicators, which can be expressed as [27]:

$$CDE = \mu_g\left(\sum F_{GT} + \sum F_{GB}\right) + CDE_{HEX} \tag{23}$$

Among them, $CDE$ is carbon dioxide emissions, $\mu_g$ is carbon dioxide emission factor of natural gas combustion, $CDE_{HEX}$ is carbon dioxide emissions of heat exchanger

3.2.4. Comprehensive Evaluation Index

Multi-objective optimization is not a single optimization goal, and finding the optimal solution for all objectives is not straightforward. To evaluate the energy system from many aspects and solve the problem that multi-objective optimization is challenging to optimize simultaneously, the weighted method is used to transform multi-objectives into a single objective, and a comprehensive evaluation system is established. To balance the contribution of every single indicator in the comprehensive evaluation system, low weight is adopted to reduce the sensitivity of a single indicator, to achieve the effect of a balanced consideration of the impact of economy, energy efficiency, and environment on the system. The specific comprehensive evaluation system is as follows:

$$HEL = \theta_1\eta_H + \theta_2\eta_E + \theta_3\eta_L \tag{24}$$

$$\eta_H = \frac{PER_{SP}}{PER_{CCHP}} \tag{25}$$

$$\eta_E = \frac{ATC_{CCHP}}{ATC_{SP}} \tag{26}$$

$$\eta_L = \frac{CDE_{SP}}{CDE_{CCHP}} \tag{27}$$

$$\theta_1 + \theta_2 + \theta_3 = 1 \tag{28}$$

where $\theta_1$, $\theta_2$ and $\theta_3$ are the weights, SP is the sub-supply system, CCHP is the triple-supply system, and the ratio of $\theta_1$, $\theta_2$ and $\theta_3$ is determined according to the inverse order of the ratio of $\eta_H$, $\eta_E$ and $\eta_L$. For example, if $\eta_H > \eta_E > \eta_L$, then $\theta_1 : \theta_2 : \theta_3 = \eta_L : \eta_E : \eta_H$.

### *3.3. Improved Ant Lion Intelligent Optimization Algorithm*

#### 3.3.1. Ant Lion Intelligent Optimization Algorithm

Mirjalili first proposed the ant lion intelligent optimization algorithm [28] in 2015, which mainly simulates the hunting mechanism of ant lion hunting ants to obtain the optimal value. The insects are called ant lions because of their unique hunting behavior and predators. Since the ALO algorithm has many advantages, such as fewer adjustment parameters and solid global searchability, it has been applied to various engineering fields [29].

In the ALO algorithm, the position of the ant is random. To describe its moving coordinates, the following (29) is used to represent the displacement of the ant in the i-dimensional space:

$$X_i(t) = [0, \cdots, cumsum(2r(t) - 1)] \tag{29}$$

$$r(t) = \begin{cases} 1, rand > 0.5 \\ 0, rand \leq 0.5 \end{cases} \tag{30}$$

Among them, $X_i(t)$ is the ant displacement, *cumsum* is the array cumulative value calculation function, $r(t)$ is the random function, *rand* is the random number, and $rand \in [0, 1]$.

In order to avoid ant search crossing the bounds, the Formula (29) is normalized and the ant search scope is limited by Formula (31):

$$R_i^t = \frac{(X_i(t) - a_i) \times (ub/I - lb/I)}{(b_i - a_i)} + \frac{lb}{I} + AL_i^{t-1} \tag{31}$$

$$I = 10^{\tau} \times \frac{t}{T} \tag{32}$$

$$\tau = \begin{cases} 2, t > 0.1T \\ 3, t > 0.5T \\ 4, t > 0.75T \\ 5, t > 0.9T \\ 6, t > 0.95T \end{cases} \tag{33}$$

where $R_i^t$ is the displacement of the ant lion or elite ant lion randomly selected by the ants around the roulette wheel and normalized, $a_i$ and $b_i$ are the minimum and maximum values in $X_i(t)$, $lb$ and $ub$ are the lower and upper bounds of the search space; $AL_i^{t-1}$ is the i-dimensional displacement of the selected ant lion; $I$ is the size of the trap range constructed by the ant lion; $\tau$ is the coefficient that increases from the initial value 1 as $t$ increases, $t$ is the current iteration number of the algorithm, and $T$ is the maximum iteration number of the algorithm.

Ant passing (34) constantly updates its position:

$$Ant_i^t = \frac{R_A^t + R_E^t}{2} \tag{34}$$

where $R_A^t$ is the position where the ants randomly walk around the lion selected by roulette, and $R_E^t$ is the position where the ants randomly walk around the elite lion.

The Ant Lion Pass (35) constantly updates its position:

$$AL_i^t = Ant_i^t, If f(Ant_i^t) > f(AL_i^t) \tag{35}$$

where $f(Ant_i^t)$ and $f(AL_i^t)$ are the fitness values of the ith-dimensional ants and ant-lion at the tth iteration, and $Ant_i^t$ and $AL_i^t$ are the positions of the ith-dimensional ants and ant lion at the tth iteration.

The specific ant lion optimization algorithm flow is shown in Figure 4.

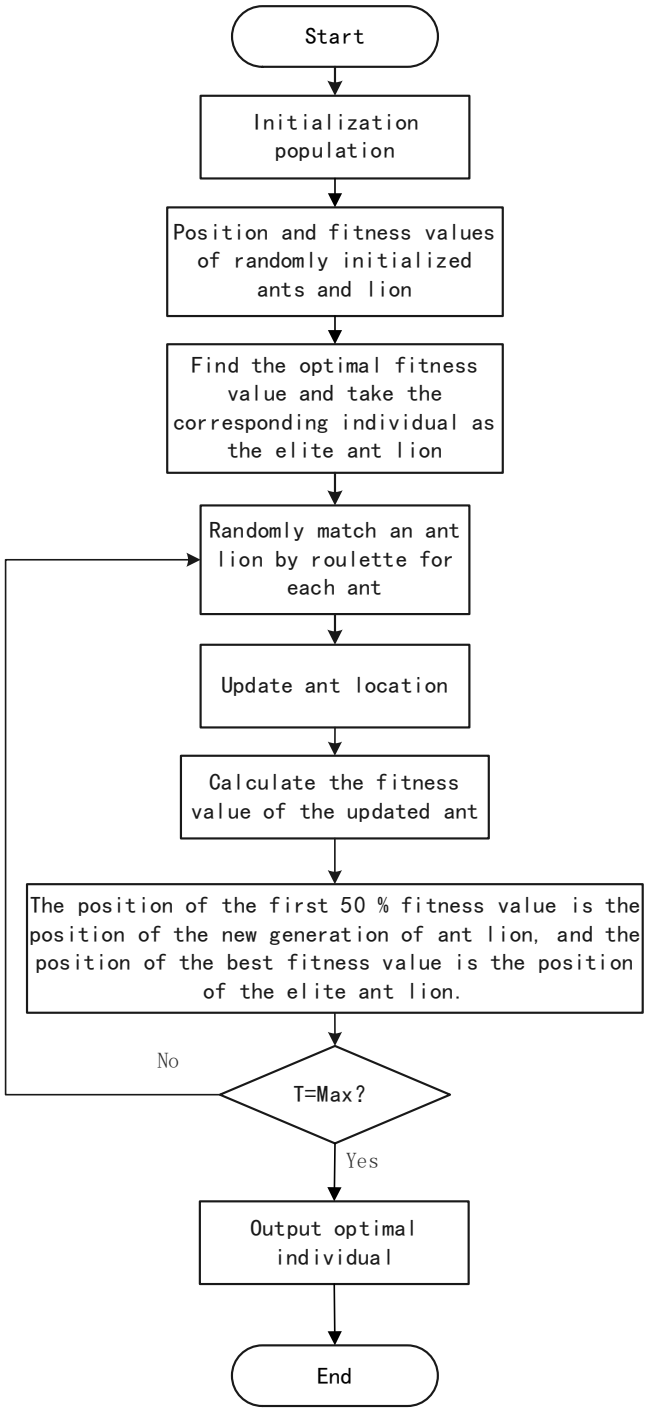


**Figure 4.** Flow chart of improved ant lion intelligent optimization algorithm.

However, the original ant lion intelligent optimization algorithm still has shortcomings, quickly falling into optimal local solution, and the solution accuracy is not high. It is necessary to improve the algorithm, optimize the performance of the algorithm, improve the accuracy of the algorithm, and prevent falling into local optimum.

3.3.2. Improved Ant Lion Intelligent Optimization Algorithm

Through the above elaboration of the original ant lion intelligent optimization algorithm, and the various standards of the actual load demand of chemical enterprises, it is necessary to improve the original ant lion intelligent optimization algorithm. The primary

purpose is to improve the algorithm's search traversal range and the algorithm's accuracy, to achieve the purpose of flexibly adjusting the system capacity configuration.

Continuous Contraction Boundary

In the ALO algorithm, the ant is 'guided' by the ant lion gradually getting close to the ant lion search stage. The boundary is gradually reduced to develop the optimal search value. The search boundary increases piecewise with the iteration of the algorithm. Although the algorithm's convergence is accelerated, the jump of the boundary value may lead to skipping some search areas and missing the optimal value.

In order to enhance the global search ability of the algorithm and enable it to traverse the solution space more comprehensively, and improve the convergence rate, a fast, smooth shrinkage formula with the iterative boundary of the algorithm is proposed, which is as follows:

$$ub/I = (ub/I)/V \tag{36}$$

$$lb/I = (lb/I)/V \tag{37}$$

$$\mathrm{V} = \psi x \frac{e^{\omega x} - e^{-\omega x}}{2} \tag{38}$$

$$\mathrm{x} = \frac{\mathrm{t}}{\mathrm{T}} \tag{39}$$

where $\psi$ and $\omega$ are the regulating factor.

Increasing Weight Coefficient

The ant population is most affected by the elite ant lions, and the 'guide' ant only swims around the elite ant macroscopically, which leads to the decrease of the ant' s traversal of the solution space, and inhibits the global search ability of the algorithm. Because of this situation, the inertia weight is increased to balance the trap gravity of elite ant lions and ant lions in different iterative periods, as follows:

$$Ant_i^t = \frac{\mu_1 \cdot R_A^t + \mu_2 \cdot R_E^t}{2} \tag{40}$$

$$\mu_1 = \cos^2\left(\frac{\pi}{2} \cdot \frac{t}{T}\right) \tag{41}$$

$$\mu_2 = \sin^2\left(\frac{\pi}{2} \cdot \frac{t}{T}\right) \tag{42}$$

where $\mu_1$ and $\mu_2$ are the weight factors, $\mu_1$ has a small proportion in the early stage of the algorithm iteration, and the guiding force of elite ant lion is small, encouraging ants to search the global solution space and improving the algorithm ergodicity, $\mu_2$. In the later stage, the ants explore and develop in the optimal region, which is beneficial to accelerate the convergence of the algorithm to the optimal value, so as to balance the local development and global search ability of the algorithm.

Improved Ant Lion Intelligent Optimization Algorithm

Through the above two improved methods, the content of the original ant lion intelligent optimization algorithm is adjusted, and the accuracy of the optimization algorithm is finally achieved.

Firstly, data initialization is carried out to determine the number and variable dimension of ants and lion, and the basic performance parameters of the core equipment are determined by inputting the three-load data of cold, heat and electricity in chemical enterprises. The capacity of the driving equipment is roughly set according to the load demand. Then, the elite ant lion is determined, and the best fitness of the initial ant lion population is selected as the elite ant lion. Then, the roulette strategy is used to select which ant lion specifically preys on an ant, and each ant can only be preyed on by an ant lion. The

higher the fitness of the ant lion, the greater the probability of capturing the ant, and the ant walks around the ant lion and the elite ant lion. Finally, the average value is taken as the position of the ants, and the fitness value of the ants and the lion is recalculated after each iteration. The position of the ants and the lion is updated according to the position and fitness value of the ants. The position of the new elite ants and the lion has the best fitness. Finally, until the end of the iteration, the optimal solution meets the conditions and the optimal individual is output. Figure 4 is the improved ant lion intelligent optimization algorithm flow chart.

### *3.4. Model Verification*

In this paper, a new type of CCHP system model is constructed by the MATLAB and based on similar structural models of other researchers, preliminary simulation and comparative analysis are carried out. In terms of system structure, the focus is on the combination of two different types of lithium bromide units and the multi-stage waste heat recovery and utilization cycle. The model building for energy storage is slightly rough, and the reliability of the structure is verified by a reference model. The results are shown in Table 1.

**Table 1.** Model verification.

| Operating and Design Conditions | This Work | Ref. [15] | Error% |
|---|---|---|---|
| Recovery efficiency of Waste Heat Boiler (%) | 0.8 | 0.8 | - |
| Power generation efficiency of Gas Turbine (%) | 0.3 | 0.3 | - |
| $CO_2$ emission (kg/kWh) | 0.22 | 0.22 | - |
| COP of Absorption Chiller | 1.3 | 1.3 | - |
| System performance | | | |
| Equipment output of Waste Heat Boiler (kW) | 325.2 | 326.8 | 0.49 |
| Equipment output of Gas Turbine (kW) | 1759 | 175.1 | 0.46 |
| Equipment output of Absorption Chiller (kW) | 559.2 | 558.5 | 0.13 |

The results show that the system output simulation under various working conditions has high accuracy, so the scheduling and optimization research based on this model has practical significance, which can guide the system's comprehensive evaluation and subsequent design improvement.

## 4. Results

In order to realize the research on the capacity configuration of the new cooling, heating, and power system proposed in this paper, a chemical enterprise in Huai'an area is selected as the research object. The main equipment parameters are referred to in Table 1. The load demand of the enterprise is divided into summer, winter, and transition seasons according to time. The leading environmental indicators are shown in Figures 5 and 6. Since the energy system studied contains photovoltaic array components, the photovoltaic output prediction is obtained by the PVsyst software simulation. The photovoltaic components applied in this study are LR4–72HPH–430M, and the inverter is PVM3–58–333–EM. Ninety groups of photovoltaic components are designed, 18 in each group. The number of components is 1620, the area occupied by the components is 3521 $m^2$, and the capacity ratio is 1.046. At the same time, the installation tilt angle, and the optimal FT (Transposition Factor) when the radiation amount is the largest, are considered; considering low power loss, and high power generation, the tilt angle is set to 27°. It can be seen from Table 2 that the highest time point of photovoltaic array power generation is 11:00 and 12:00. The daily power generation in April and May is relatively higher throughout the year. The output status of the photovoltaic array is shown in Table 2.

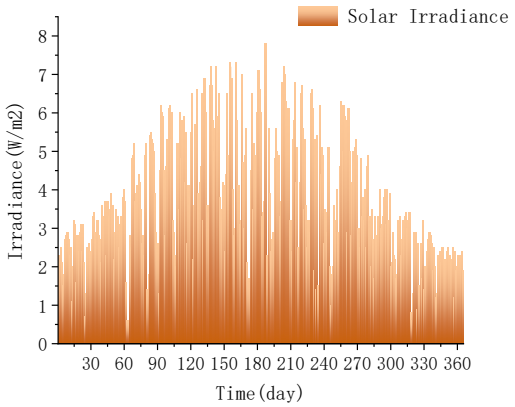


**Figure 5.** Annual solar irradiance.

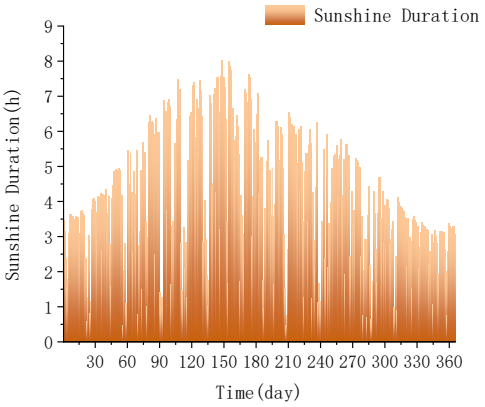


**Figure 6.** Annual sunshine duration.

**Table 2.** Monthly hourly average of PV array output (kW).

| Month | 1H | 2H | 3H | 4H | 5H | 6H | 7H | 8H | 9H | 10H | 11H | 12H |
|---|---|---|---|---|---|---|---|---|---|---|---|---|
| 1 | 0 | 0 | 0 | 0 | 0 | 0 | 3 | 109 | 205 | 268 | 314 | 300 |
| 2 | 0 | 0 | 0 | 0 | 0 | 0 | 33 | 119 | 227 | 296 | 360 | 374 |
| 3 | 0 | 0 | 0 | 0 | 0 | 3 | 65 | 149 | 223 | 279 | 326 | 335 |
| 4 | 0 | 0 | 0 | 0 | 0 | 36 | 110 | 202 | 272 | 336 | 358 | 364 |
| 5 | 0 | 0 | 0 | 0 | 5 | 57 | 135 | 216 | 298 | 340 | 364 | 350 |
| 6 | 0 | 0 | 0 | 0 | 13 | 49 | 109 | 187 | 252 | 308 | 319 | 289 |
| 7 | 0 | 0 | 0 | 0 | 3 | 42 | 107 | 174 | 245 | 282 | 307 | 320 |
| 8 | 0 | 0 | 0 | 0 | 0 | 32 | 88 | 155 | 227 | 281 | 306 | 307 |
| 9 | 0 | 0 | 0 | 0 | 0 | 28 | 107 | 203 | 274 | 323 | 350 | 353 |
| 10 | 0 | 0 | 0 | 0 | 0 | 3 | 84 | 163 | 235 | 290 | 305 | 312 |
| 11 | 0 | 0 | 0 | 0 | 0 | 0 | 54 | 146 | 220 | 266 | 291 | 257 |
| 12 | 0 | 0 | 0 | 0 | 0 | 0 | 17 | 112 | 193 | 285 | 306 | 312 |
| **Month** | **13H** | **14H** | **15H** | **16H** | **17H** | **18H** | **19H** | **20H** | **21H** | **22H** | **23H** | **24H** |
| 1 | 282 | 230 | 142 | 51 | 0 | 0 | 0 | 0 | 0 | 0 | 0 | 0 |
| 2 | 343 | 279 | 197 | 97 | 4 | 0 | 0 | 0 | 0 | 0 | 0 | 0 |
| 3 | 291 | 236 | 151 | 77 | 20 | 0 | 0 | 0 | 0 | 0 | 0 | 0 |
| 4 | 350 | 299 | 223 | 128 | 46 | 0 | 0 | 0 | 0 | 0 | 0 | 0 |
| 5 | 327 | 288 | 211 | 135 | 56 | 6 | 0 | 0 | 0 | 0 | 0 | 0 |
| 6 | 272 | 218 | 162 | 109 | 49 | 15 | 0 | 0 | 0 | 0 | 0 | 0 |
| 7 | 297 | 242 | 187 | 115 | 57 | 15 | 0 | 0 | 0 | 0 | 0 | 0 |
| 8 | 288 | 251 | 179 | 104 | 47 | 3 | 0 | 0 | 0 | 0 | 0 | 0 |
| 9 | 330 | 261 | 188 | 99 | 21 | 0 | 0 | 0 | 0 | 0 | 0 | 0 |
| 10 | 292 | 217 | 141 | 58 | 1 | 0 | 0 | 0 | 0 | 0 | 0 | 0 |
| 11 | 239 | 180 | 103 | 17 | 0 | 0 | 0 | 0 | 0 | 0 | 0 | 0 |
| 12 | 282 | 202 | 108 | 7 | 0 | 0 | 0 | 0 | 0 | 0 | 0 | 0 |

According to the improved ant lion intelligent algorithm proposed in this paper, the research object is solved according to the above steps, and the cooling, heating, and power operation conditions of typical summer days, winter days, and transition seasons of the enterprise, are obtained. The specific results are shown in Figures 7–15. According to the comprehensive evaluation system proposed in this paper, the research system is solved, and the results are shown in Figure 16.

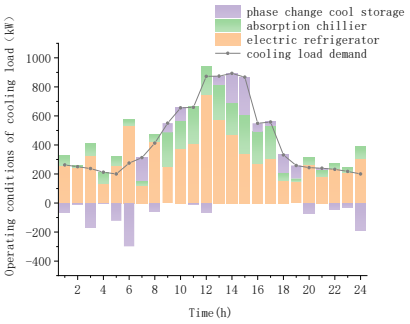


**Figure 7.** Typical daily cooling conditions in summer.

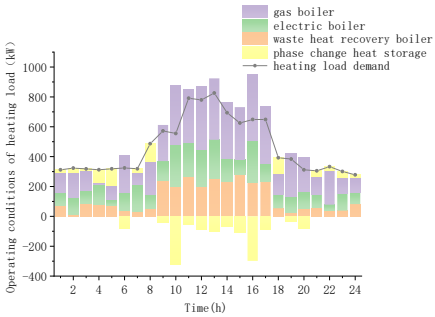


**Figure 8.** Typical daily heating conditions in summer.

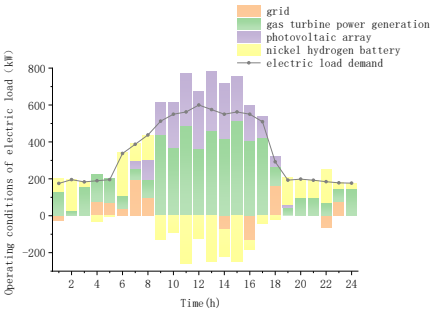


**Figure 9.** Typical daily power operation conditions in summer.

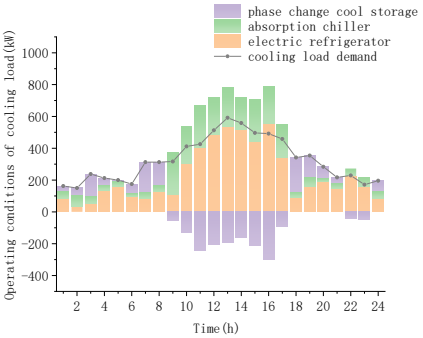


**Figure 10.** Typical daily cooling conditions in winter.

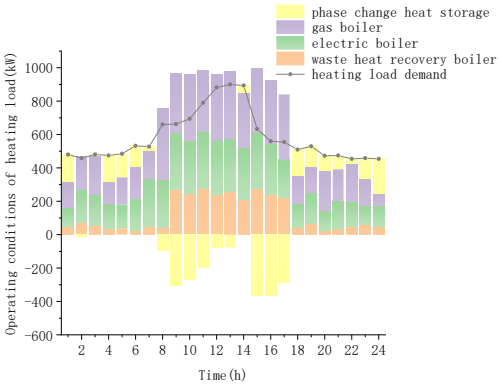


**Figure 11.** Typical daily heating conditions in winter.

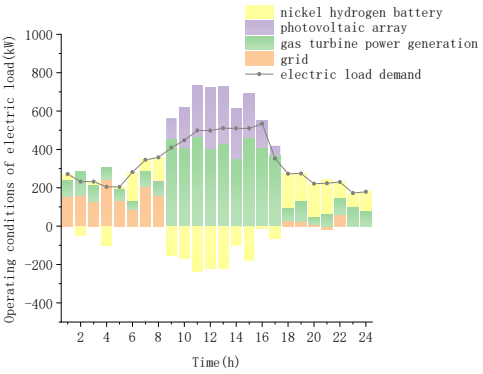


**Figure 12.** Typical daily and power operation conditions in winter.

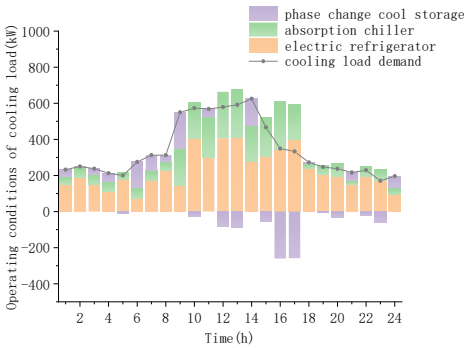


**Figure 13.** Typical daily cooling conditions in the transition season.

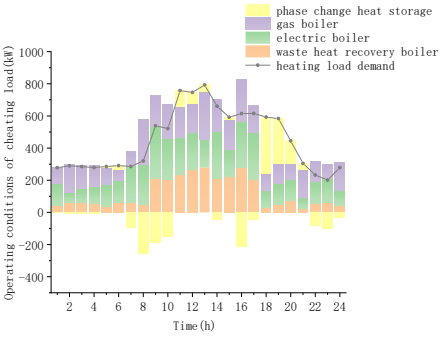


**Figure 14.** Typical daily heating conditions in the transition season.

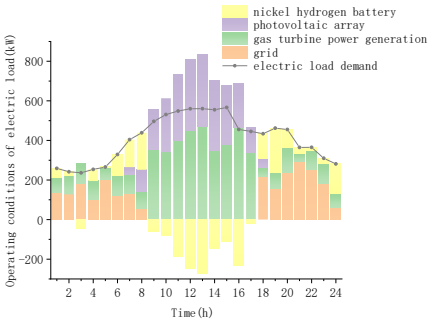


**Figure 15.** Typical daily power operation conditions in the transition season.

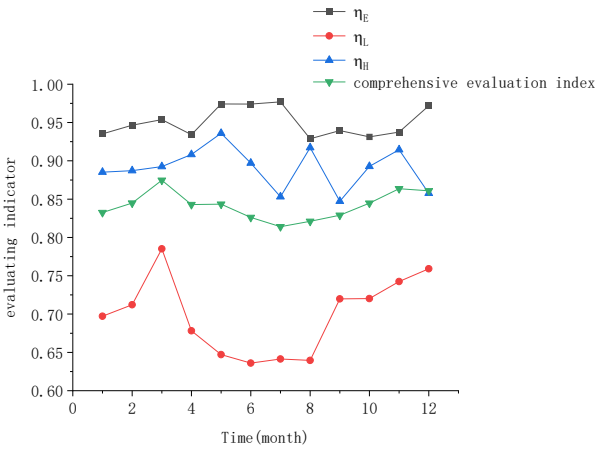


**Figure 16.** Comprehensive evaluation system diagram.

According to Figures 7–9, it can be found that the cooling load demand of the selected chemical enterprises is the highest, but due to the particularity of chemical enterprises, the heating demand is also high in summer, the electricity demand is relatively low, and the load demand of all-day working hours is relatively high. The cooling load demand reaches the peak from 12:00 to 15:00, and the peak is 893 kW at 14:00. The heating load demand reaches the peak from 11:00 to 13:00, and the peak is 826 kW at 13:00. The electric load is at the high load demand level from 9:00 to 17:00, and the peak is 600 kW at 12:00. The cooling load demand of the enterprise is provided by two absorption lithium bromide chillers and electric refrigerators. In the working time, the cooling load demand is higher, the output of two refrigeration equipment is higher, and the electric refrigerator undertakes more heavy cooling output. The output of the whole day is more than 200 kW, and the maximum is 748.016 kW. It belongs to the peak range of the cooling load demand on the day. In the case of non-working time, multiple cooling loads are stored while meeting the cooling load demand. The heating load of the enterprise is provided by gas boiler, electric boiler, and waste heat boiler, and the priority of the gas boiler and waste heat boiler using process heating is higher than that of electric boiler. The electric boiler plays the role of auxiliary boiler, and the gas boiler supplies the biggest part of the heating load. The output of the gas boiler is more than 400 kW in the working time of the enterprise, and the highest heating generation rate is 419.567 kW, which belongs to the peak range of the heating load demand on the day. The power load of the enterprise is provided by the gas turbine power generation device, photovoltaic, and power grid. The solar irradiance is high at noon in summer, and the output of photovoltaic modules is high. The photovoltaic output is more than 200 kW from 10 to 15, and the highest output point is 320 kW at 13. Gas turbine is the main power supply equipment, and the output is more than 300 kW from 9 to 17. It provides about 80% of the electricity demand in this period, and the highest point is 513.667 kW at 15. The power grid buys electricity in the valley to meet the electricity demand of the enterprise.

According to Figures 10–12, it can be found that the winter heating load demand of chemical enterprises is the highest, and the demand is higher than that of the summer cooling load. The winter cooling load demand is relatively low. The cooling load demand from 9:00 to 14:00 is in the peak range of winter cooling load demand, and the highest point is 13:00 to 519 kW. The heating load is in the peak range of heating load demand from 12:00 to 14:00, and the highest point is 13:00 to 899 kW, which is higher than the summer cooling load demand. The electric load demand is slightly lower than typical summer days, and the highest point is 16:00 to 16:00, which is 534 kW. The absorption lithium bromide chiller cannot meet the cooling load demand of the enterprise by using the process heating refrigerating capacity. The electric refrigerator is the central cooling equipment. The output of the electric refrigerator from 10 o'clock to 17 o'clock is higher than 300 kW, which provides about 75% of the cooling load. While meeting the cooling load demand, the cooling load is stored for the non-working period. The heating load demand of the enterprise is high, and the output of the gas boiler and the electric boiler equipment is high. The output of the gas boiler is up to 399.893 kW at 13 o'clock. The output of the electric boiler is improved compared with the summer, and the highest point is 100 kW to meet the higher heating load demand. In winter, the highest point of the electric boiler is 340.387 kW at 11 o'clock, and the output of the working time is higher. Due to the particularity of the enterprise, the load demand is higher, and the output of the heating equipment is also improved. The electricity demand of enterprises has no significant difference compared to that in summer, mainly provided by the gas turbine power generation device. Additionally, about 80 % of the electricity load is provided from 9:00 to 17:00. When meeting the electricity demand, the electricity is stored for the electricity demand in the non-working period. The output of photovoltaic modules is lower than in summer, and the highest point is up to 300 kW at 13:00. The electricity purchase in valley time meets the electricity demand.

According to Figures 13–15, the heating load demand of enterprises is still the highest, and the electricity demand is low. The demand during the transition season is low, and equipment output during working hours is reduced. The cooling load is in a relatively high range from 9:00 to 14:00, and the highest point is 625 kW at 14:00, which is 30.01% lower than in summer. The heating load is in a high demand range from 11:00 to 13:00, and the highest point is 792 kW at 13:00, which is 11.9% lower than in the winter. The electricity load is in a high demand range from 11:00 to 1:00, and the highest point is 567 kW at 15:00, which has a small gap from the highest point, which shows the difference between the winter and summer. The output of electric refrigerators is lower than that in winter and summer. The highest output of electric refrigerators in the transition season is 409.94 kW at 13:00, which is 45.19% lower than in summer and 23.8% lower than in winter. The output of the lithium bromide refrigeration unit is almost the same, and the output of the electric refrigerator is relatively improved during non-working hours. The heating load demand is relatively low in the transition season, the output of the gas boiler is reduced, and the highest point is 297.67 kW at 13:00, which is 27.71% lower than the highest point in summer and 25.56% lower than the highest point in winter. There is little difference in the heating supply between waste heat boilers in winter and summer, and the heating storage of the system is less. In the transition season, the gas turbine output is relatively low in the non-working period, the power generation is reduced, and the electricity storage of the system is reduced. It is more dependent on purchasing electricity from the power grid, which is twice that of purchasing electricity in winter.

As a driving device, the capacity configuration of a gas turbine should not be too high, and the cooling capacity and heating capacity generated by heating utilization cannot meet their individual needs. Therefore, other energy supply equipment should be matched to configure the capacity flexibly.

According to Figure 16, it can be found that from the comprehensive evaluation system curve, the comprehensive performance of the summer system is the best, and the best is 0.814 in July, while the comprehensive performance of the transition season system is

relatively low, and the worst is 0.875 in March. From the point of view of each sub-index, due to the diversification of the equipment collocation and the complexity of the way of the research, the annual cost of the typical cooling-thermal power system is almost the same. Carbon dioxide emissions are positively correlated with primary energy utilization. In summer, the thermal cascade utilization is complex, the utilization rate is higher, the carbon dioxide emissions are lower, and the performance is better. In terms of carbon dioxide emissions, the best advantage of the structure-optimized CCHP system was 119030.11 in July, and the indicator in the comprehensive evaluation system was 0.641, but the best advantage of carbon dioxide emissions was 0.636 in June. In terms of primary energy utilization, the best advantage of the structure-optimized CCHP system was 75.87% in July, and the indicator in the comprehensive evaluation system was 0.853.

## 5. Conclusions

In this paper, an improved ant lion optimization algorithm is proposed to optimize the capacity configuration of the new CCHP system. Taking a chemical enterprise in Huai'an as an example, considering the particularity of the production process of the chemical enterprise, the annual operating conditions of the system and the overall comprehensive performance of the system are analyzed. In this system, an intelligent optimization algorithm is used to improve the rationality of system equipment capacity configuration and maximize the role of the energy supply system. The system analysis shows that the optimized CCHP system has better performance in economic, energy, and environmental benefits, and the overall comprehensive evaluation system has better results.

(1) The annual operating conditions of the new energy system proposed in this paper are excellent, and the annual cost index is the lowest at CNY 5.155 million on typical summer days. The minimum carbon dioxide emissions are 119030.11 kg, and the highest primary energy utilization rate was 75.87% on typical winter days. The minimum annual cost index is CNY 5859 million. The minimum carbon dioxide emissions are 142854.91 kg. At the same time, the highest primary energy utilization rate was 71.86% on the typical days of the transition season. The minimum annual cost index is CNY 5335 million. The minimum carbon dioxide emissions are 120724.29 kg, and the highest primary energy utilization rate was 74.9%.

The results show the system can fully supply the multi-load with low cost and high efficiency.

(2) The comprehensive evaluation system adopted in this paper is composed of annual cost, primary energy utilization rate, and carbon dioxide emissions. The coupling adopts the method of adding weights. The selection of weights considers the contribution of each index. When applied to the research object, the optimal comprehensive index can reach 0.814.

(3) The modelling and simulation results show that the ant lion optimization algorithm can improve the rationality of the capacity allocation of the system equipment. Compared with the typical CCHP system, the performance of the CCHP system with structural optimization is better. The summer performance is the best for the system's annual operation. Specifically, in terms of annual cost, the annual cost savings of the new structural system are up to 13%. The unique structural system has a maximum reduction of 36.39% in carbon dioxide emissions. In terms of primary energy utilization, the primary energy utilization rate of the new structural system increases by up to 18%. The overall comprehensive evaluation system is up to 0.814.

**Author Contributions:** Methodology, T.P.; formal analysis, R.G.; investigation, H.H., J.Z. and M.S.N.; writing—original draft preparation, F.W.; writing—review and editing, M.Z., C.Z. and J.H.; supervision, Y.W.; project administration, J.J.; funding acquisition, R.J.; All authors have read and agreed to the published version of the manuscript.

**Funding:** Jiangsu Provincial Department of Education: 21KJD480001.

**Institutional Review Board Statement:** Not applicable.

**Informed Consent Statement:** Not applicable.

**Data Availability Statement:** Data will be made available on request.

**Conflicts of Interest:** The authors declare no conflict of interest.

## Nomenclature

| | |
|---|---|
| GT | Gas Turbine |
| EC | Electric Refrigerator |
| AC.W | Waste heat lithium bromide absorption chiller |
| AC.S | Steam dual-effect lithium bromide absorption chiller |
| WHRB | Waste Heat Recovery Boiler |
| PV | Photovoltaic Array |
| EB | Electric Boiler |
| HEX | Heat Exchanger |
| ATC | Annual Cost |
| PER | Primary Energy Ratio |
| CDE | Carbon Dioxide Emissions |
| HEL | Comprehensive Evaluation Index |

## References


1. Sun, S.; Yu, C.; Sun, T.; Li, X.; Wei, Y.; Tan, J.; Zhang, J. Research Progress of CCHP Distributed Energy System. *Water Conserv. Electr. Power Mach.* **2019**, *41*, 7.
2. Meng, X.; Nan, Z.; Li, B.; Feng, H. Design and Energy Analysis of CCHP System Based on Natural Gas Internal Combustion Engine Generator Set. *Energy Conserv.* **2019**, *38*, 4.
3. Li, Z.; Li, W.; Zhao, J.; Shan, D. Parameter optimization and comprehensive analysis of biomass-driven ORC triple supply system. *Acta Energ. Sol. Sin.* **2020**, *41*, 7.
4. Zhang, X.; Ge, L.; Gao, B.; Zhang, S. Joint Optimization and Ideal Fuzzy Decision Method of CCHP and Distributed Photovoltaic System. *J. Henan Polytech. Univ. Nat. Sci.* **2020**, *39*, 7.
5. Wei, Z.; Gen, Y.; Chi, F.; Sun, K. Photovoltaic Capacity Configuration of CCHP System Based on Niche and Fuzzy Ideal Decision. *J. Yanshan Univ.* **2019**, *43*, 8.
6. Ji, J.; Xia, X.; Ni, W.; Teng, K.; Miao, C.; Wang, Y.; Roskilly, T. An Experimental and Simulation Study on Optimisation of the Operation of a Distributed Power Generation System with Energy Storage—Meeting Dynamic Household Electricity Demand. *Energies* **2019**, *12*, 1091. [CrossRef]
7. Zhang, T.; Hu, Z.; Zhang, D. Capacity Configuration Optimization of Building Integrated Energy System. *Electr. Power Constr.* **2019**, *40*, 3–11.
8. Li, W.; Guan, Y.; Chen, C.; Cai, L.; Yang, Y. Study on Capacity Configuration Optimization of CCHP System in Office Building. In Proceedings of the Conference Paper Report of Heating Engineering Construction and Efficient Operation Seminar, Zhejiang, China, 25–27 October 2017.
9. Xu, J.; Yao, Y.; Yousefi, N. Optimal prime mover size determination of a CCHP system based on 4E analysis. *Energy Rep.* **2021**, *7*, 4376–4387. [CrossRef]
10. Wu, D.; Han, Z.; Liu, Z.; Zhang, H. Study on configuration optimization and economic feasibility analysis for combined cooling, heating and power system. *Energy Convers. Manag.* **2019**, *190*, 91–104. [CrossRef]
11. Wang, M.; Zhao, X.; Heidari, A.A.; Chen, H. Evaluation of constraint in photovoltaic models by exploiting an enhanced ant lion optimizer. *Sol. Energy* **2020**, *211*, 503–521. [CrossRef]
12. Wang, M.; Heidari, A.A.; Chen, M.; Chen, H.; Zhao, X.; Cai, X. Exploratory differential ant lion-based optimization. *Expert Syst. Appl.* **2020**, *159*, 113548. [CrossRef]
13. Rani, R.; Garg, R. Pareto based ant lion optimizer for energy efficient scheduling in cloud environment. *Appl. Soft Comput.* **2021**, *113*, 107943. [CrossRef]
14. Li, Q.; Li, D.; Zhao, K.; Wang, L.; Wang, K. State of health estimation of lithium-ion battery based on improved ant lion optimization and support vector regression. *J. Energy Storage* **2022**, *50*, 104215. [CrossRef]
15. Chen, P.; Sun, K.; Zhang, C.; Sun, B. A Feasible Zone Analysis Method with Global Partial Load Scanning for Solving Power Flow Coupling Models of CCHP Systems. *J. Mod. Power Syst. Clean Energy* **2022**, *10*, 7. [CrossRef]
16. Mianaei, P.K.; Aliahmadi, M.; Faghri, S.; Ensaf, M.; Ghasemi, A.; Abdoos, A.A. Chance-Constrained Programming for Optimal Scheduling of Combined Cooling, heating, and Power-based Microgrid Coupled with Flexible Technologies. *Sustain. Cities Soc.* **2021**, *77*, 103502. [CrossRef]
17. Cao, Y.; Wang, Q.; Wang, Z.; Jermsittiparsert, K.; Shafiee, M. A new optimized configuration for capacity and operation improvement of CCHP system based on developed owl search algorithm. *Energy Rep.* **2020**, *6*, 315–324. [CrossRef]

18. Wang, A.; Wang, S.; Ebrahimi-Moghadam, A.; Farzaneh-Gord, M.; Moghadam, A.J. Techno-economic and techno-environmental assessment and multi-objective optimization of a new CCHP system based on waste heat recovery from regenerative Brayton cycle. *Energy* **2022**, *241*, 122521. [CrossRef]
19. Lu, C.; Wang, J.; Yan, R. Multi-objective optimization of combined cooling, heating and power system considering the collaboration of thermal energy storage with load uncertainties. *J. Energy Storage* **2021**, *40*, 102819. [CrossRef]
20. Wang, Z.; Cai, W.; Tao, H.; Wu, D.; Meng, J. Research on capacity and strategy optimization of combined cooling, heating and power systems with solar photovoltaic and multiple energy storage. *Energy Convers. Manag.* **2022**, *268*, 115965. [CrossRef]
21. Ji, J.; Ding, Z.; Xia, X.; Wang, Y.; Huang, H.; Zhang, C.; Peng, T.; Wang, X.; Nazir, M.S.; Zhang, Y.; et al. System Design and Optimisation Study on a Novel CCHP System Integrated with a Hybrid Energy Storage System and an ORC. *Complexity* **2020**, *2020*, 1278751. [CrossRef]
22. Zhang, D.; Ma, Y.; Liu, J.; Jiang, S.; Chen, Y.; Wang, L.; Zhang, Y.; Li, M. Stochastic Optimization Method for Energy Storage System Configuration Considering Self-Regulation of the State of Charge. *Sustainability* **2022**, *14*, 553. [CrossRef]
23. Yang, X.; Liu, K.; Leng, Z.; Liu, T.; Zhang, L.; Mei, L. Multi-dimensions analysis of solar hybrid CCHP systems with redundant design. *Energy* **2022**, *253*, 124003. [CrossRef]
24. Melo, F.M.; Magnani, F.S.; Carvalho, M. A decision-making method to choose optimal systems considering financial and environmental aspects: Application in hybrid CCHP systems. *Energy* **2022**, *250*, 123816. [CrossRef]
25. Yan, R.; Wang, J.; Wang, J.; Tian, L.; Tang, S.; Wang, Y.; Zhang, J.; Cheng, Y.; Li, Y. A two-stage stochastic-robust optimization for a hybrid renewable energy CCHP system considering multiple scenario-interval uncertainties. *Energy* **2022**, *247*, 123498. [CrossRef]
26. Zhang, Y.; Sun, H.; Tan, J.; Li, Z.; Hou, W.; Guo, Y. Capacity configuration optimization of multi-energy system integrating wind turbine/photovoltaic/hydrogen/battery. *Energy* **2022**, *252*, 124046. [CrossRef]
27. Mehregan, M.; Abbasi, M.; Khalilian, P.; Hashemian, S.M.; Madadi, A. Energy, economic, environmental investigations and optimization of a combined cooling, heating and power system with hybrid prime mover of gas engine and flat plate solar collector. *Energy Convers. Manag.* **2022**, *251*, 115018. [CrossRef]
28. Mirjalili, S. The Ant Lion Optimizer. *Adv. Eng. Softw.* **2015**, *83*, 80–98. [CrossRef]
29. Li, Z.; Wu, W.; Lin, Z. An image enhancement method using improved ant-lion optimization algorithm. *Appl. Res. Comput.* **2018**, *35*, 4.